

Spectral characteristics of laser-plasma instabilities with a broadband laser

Guo-Xiao Xu(许国潇), Ning Kang(康宁), An-Le Lei(雷安乐), Hui-Ya Liu(刘会亚), Yao Zhao(赵耀), Shen-Lei Zhou(周申蕾), Hong-Hai An(安红海), Jun Xiong(熊俊), Rui-Rong Wang(王瑞荣), Zhi-Yong Xie(谢志勇), Xi-Chen Zhou(周熙晨), Zhi-Heng Fang(方智恒), and Wei Wang(王伟)

Citation: Chin. Phys. B, 2024, 33 (**8**): 085204. DOI: 10.1088/1674-1056/ad426d

What follows is a list of articles you may be interested in

Model of self-generated magnetic field generation from relativistic laser interaction with solid targets

Rui Yan(严睿), De-Bin Zou(邹德滨), Na Zhao(赵娜), Xiao-Hu Yang(杨晓虎), Xiang-Rui Jiang(蒋祥瑞), Li-Xiang Hu(胡理想), Xin-Rong Xu(徐新荣), Hong-Yu Zhou(周泓宇), Tong-Pu Yu(余同普), Hong-Bin Zhuo(卓红斌), Fu-Qiu Shao(邵福球), and Yan Yin(银燕)

Chin. Phys. B, 2024, 33 (**5**): 055203. DOI: 10.1088/1674-1056/ad333f

Transmission effects of high energy nanosecond lasers in laser-induced air plasma under different pressures

Wei-Min Hu(胡蔚敏), Kai-Xin Yin(尹凯欣), Xiao-Jun Wang(王小军), Jing Yang(杨晶), Ke Liu(刘可), Qin-Jun Peng(彭钦军), and Zu-Yan Xu(许祖彦)

Chin. Phys. B, 2023, 32 (**10**): 105201. DOI: 10.1088/1674-1056/acb0bf

Nonlinear mixing-based terahertz emission in inclined rippled density plasmas

K Gopal, A P Singh, and S Divya

Chin. Phys. B, 2023, 32 (**6**): 065202. DOI: 10.1088/1674-1056/aca9c9

Intense low-noise terahertz generation by relativistic laser irradiating near-critical-density plasma

Shijie Zhang(张世杰), Weimin Zhou(周维民), Yan Yin(银燕), Debin Zou(邹德滨), Na Zhao(赵娜), Duan Xie(谢端), and Hongbin Zhuo(卓红斌)

Chin. Phys. B, 2023, 32 (**3**): 035201. DOI: 10.1088/1674-1056/ac872c

Correction of intense laser-plasma interactions by QED vacuum polarization in collision of laser beams

Wen-Bo Chen(陈文博) and Zhi-Gang Bu(步志刚)

Chin. Phys. B, 2023, 32 (**2**): 025204. DOI: 10.1088/1674-1056/ac70b3

Spectral characteristics of laser-plasma instabilities with a broadband laser

Guo-Xiao Xu(许国潇)[1,4], Ning Kang(康宁)[1,†], An-Le Lei(雷安乐)[2,‡], Hui-Ya Liu(刘会亚)[1], Yao Zhao(赵耀)[3], Shen-Lei Zhou(周申蕾)[1], Hong-Hai An(安红海)[2], Jun Xiong(熊俊)[2], Rui-Rong Wang(王瑞荣)[2], Zhi-Yong Xie(谢志勇)[2], Xi-Chen Zhou(周熙晨)[2], Zhi-Heng Fang(方智恒)[2], and Wei Wang(王伟)[2]

[1] *Key Laboratory of High Power Laser and Physics, Shanghai Institute of Optics and Fine Mechanics, Chinese Academy of Sciences, Shanghai* 201800, *China*

[2] *Shanghai Institute of Laser Plasma, China Academy of Engineering Physics, Shanghai* 201800, *China*

[3] *School of Science, Shenzhen Campus of Sun Yat-sen University, Shenzhen* 518107, *China*

[4] *University of Chinese Academy of Sciences, Beijing* 100049, *China*

(Received 5 March 2024; revised manuscript received 10 April 2024; accepted manuscript online 24 April 2024)

Recent experimental progresses regarding broadband laser-plasma instabilities (LPIs) show that a 0.6% laser bandwidth can reduce backscatters of the stimulated Brillouin scattering (SBS) and the stimulated Raman scattering (SRS) at normal incidence [*Phys. Rev. Lett.* **132** 035102 (2024)]. In this paper, we present a further discussion of the spectral distributions of the scatters developed by broadband LPIs, in addition to a brief validation of the effectiveness of bandwidth on LPIs mitigation at oblique incidence. SBS backscatter has a small redshift in the broadband case contrary to the blueshift with narrowband laser, which may be explained by the self-cross beam energy transfer between the various frequency components within the bandwidth. SRS backscatter spectrum presents a peak at a longer wavelength in the broadband case compared to the short one in the narrowband case, which is possibly attributed to the mitigation effect of bandwidth on filaments at underdense plasmas. The three-halves harmonic emission ($3\omega/2$) has a one-peak spectral distribution under the broadband condition, which is different from the two-peak distribution under the narrowband condition, and may be related to the spectral mixing of different frequency components within the bandwidth if the main sources of the two are both two-plasmon decays.

Keywords: laser-plasma instability, laser bandwidth, light spectrum

PACS: 52.38.–r, 52.57.–z, 52.38.Bv **DOI:** 10.1088/1674-1056/ad426d

1. Introduction

In direct-drive inertial confinement fusion (DDICF), the laser directly heats the outer ablative layer, creating an inward ablative pressure that drives fuel compression and eventually a thermonuclear reaction.[1,2] Under ideal conditions, the thermonuclear reaction will achieve self-sustaining burn by α-heating. The ablation pressure and the implosion velocity determine the implosion performance, which depends on the effective deposition of laser energy into the target capsule and the maintenance of the compressibility of the fuel. However, ablation creates a low-density plasma corona that excites a variety of laser-plasma instabilities (LPIs), potentially reducing implosion performance.[3] LPIs, on the one hand, reduce energy deposition by scattering light, and on the other hand generate hot electrons to preheat cold fuel, reducing compressibility and seriously hindering the goal of high-gain ignition. LPI in direct drive mainly includes three single-beam instabilities,[4] namely, stimulated Raman scattering (SRS), stimulated Brillouin scattering (SBS), and two-plasmon decay (TPD), as well as multi-beam instabilities,[5] such as cross-beam energy transfer (CBET). Among them, SRS and TPD produce hot electrons[6] pointing to low-temperature fuel, which will preheat it and therefore increase entropy. SBS and CBET produce intense scatters, resulting in considerable energy loss and seriously affecting the deposition of energy.[5] Therefore, how to effectively suppress LPIs is an important problem for DDICF.

LPI suppression can be achieved based on the controls of both laser and plasma, in which using a broadband laser to suppress LPIs is a hot spot in DDICF research.[7–16] Early theoretical studies have suggested that LPI could be effectively suppressed when the laser bandwidth is much larger than its growth rate. For example, Lu[13] found that the bandwidth could significantly increase the threshold of absolute SRS and TPD. More detailed studies revealed the principles of LPI suppression by laser bandwidth, including detuning the interaction between waves (such as CBET),[11] incoherently driving many small instabilities to replace a single strong one (such as TPD),[15] and inducing time-incoherently interrupted excitation of plasma waves. In recent years, great progress has been made in broadband laser techniques,[17–19] and many broadband laser schemes have been proposed,[14,20–24] but most of them are established on the basis of large bandwidth. Due to the technical and engineering limitations of existing laser fa-

†Corresponding author. E-mail: kangning@siom.ac.cn

‡Corresponding author. E-mail: lal@siom.ac.cn

© 2024 Chinese Physical Society and IOP Publishing Ltd

cilities, they can hardly meet the requirement on such a level of bandwidth, so the schemes mostly stay in the theoretical and simulation stages.

Based on a more practical bandwidth level, Follett *et al.*[25] recently conducted a numerical study on the absolute instability threshold of SRS and TPD with broadband laser. Their calculations showed that the absolute instability threshold can be significantly increased when the relative bandwidth is $\sim 1\%$, and an approximate threshold formula under such broadband conditions is proposed. Follett *et al.*[26] further developed the broadband LPI theory, suggesting that a 1.6% bandwidth can adequately suppress SRS backscattering at the ignition scale. Liu *et al.*[27] used particle-in-cell simulation to study the evolution of SRS backscatter driven by multi-frequency (multi-color) laser, and found that the increase of laser incoherence to 0.5% would cause SRS backscatter to enter a nonlinear evolution stage, resulting in intermittent bursts. They further predicted that SRS backscattering will be greatly suppressed if the bandwidth reaches more than 2.5%. In short, many theoretical studies have shown that laser bandwidth of less than 1% also has significant impacts on LPIs, but the idea was not confirmed by any experiment for years due to the lack of appropriate laser conditions.

Recent experimental progress has been made at the Kunwu laser facility,[28] which provides one green laser beam with a bandwidth as large as 0.6%. Measurements of the scatters induced by LPIs showed that a 0.6%-bandwidth can mitigate LPIs to a certain extent at normal incidence, especially for the SBS backscattering.[29] In this paper, we present further discussion on the spectral distributions (shapes) of the scatters developed by broadband LPIs, in addition to a brief validation of the effectiveness of bandwidth on LPIs mitigation at oblique incidence. This paper is organized as follows. Section 2 describes the design and the main parameters of the experiments. Section 3 introduces the experimental results and discusses the reasons for the changes in scatters under broadband conditions in terms of spectral distribution. The conclusion and perspectives are drawn in Section 4.

2. Experimental setup

Figure 1(a) shows the setup of the experiments, which were carried out at the Kunwu broadband laser facility.[19,28] 3.2-ns, 0.53-μm (λ) laser pulses applied with a continuous phase plate (CPP) irradiate planar targets within a spot size of about 180 μm normally and obliquely (30°). The lasers are polarized in the direction perpendicular to the diagnostic plane (i.e., the view plane of Fig. 1(a)). For oblique incidence, the targets are rotated in the diagnostic plane, so the incident lasers are S-polarized. Two laser bandwidths are included in the experiments, namely, narrowband and broadband, and their typical spectra are shown in Fig. 1(b). The narrowband laser is the second harmonic of a conventional neodymium glass laser, whose bandwidth is extremely small so that it can be roughly treated as monochromatic. The fundamental broadband laser is an amplified superluminescent pulse in a neodymium glass amplifier, which is then converted to a second harmonic resulting in a green broadband laser with 3.2 nm bandwidth (full width at half maximum).[30,31] The broadband spectrum roughly fits a Lorentzian function, so its coherence time satisfies $\tau_c \Delta\omega \approx 2$, where $\Delta\omega$ is the bandwidth in angular frequency.[25] The f-number ($f_\#$) of the laser beam is 4.2. Targets are 30-μm-thick plastic (CH) and 15-μm-thick titanium (Ti) bilayer planar targets, in which CH is the layer irradiated by the laser beam.

Spectral diagnostics of the experiments cover SBS and SRS backscatters and the three-halves harmonic emission ($3\omega/2$) scatters at various angles from 90° to 170°, where 0° refers to the laser incidence. $3\omega/2$ scatters are collected by fiber probes inside the target chamber, while the backscatters are concentrated to a diffuser at laser backward outside the chamber before they are collected by fibers. The spectrometer for $3\omega/2$ has a 0.1-nm resolution, and that for the backscatters covers both the SBS and SRS bands with a 1.7-nm resolution. The calculation of scattering energy based on calibration using a standard light source has an uncertainty of about ±20%.

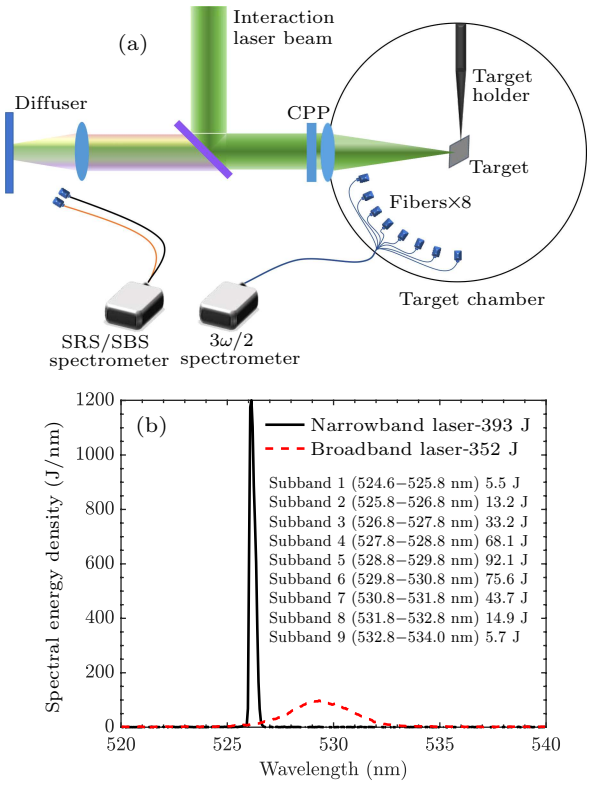


Fig. 1. Experimental conditions. (a) Schematic diagram of the experimental setup. (b) Narrowband and broadband laser spectra at 350–400 J energies. The center wavelength of the narrowband laser is 526.1 nm, and that of the broadband laser is 529.3 nm. The relative bandwidth ($\Delta\omega/\omega_0$, where ω_0 refers to the center angular frequency of the laser) of the broadband laser is about 0.6%. The energy proportion within each wavelength range (sub-band) of the broadband laser is shown in the upper right corner.

3. Results and discussion

A comparison between normal and oblique incidences at ~ 230 J incident energy corresponding to an average intensity of $\sim 2.8 \times 10^{14}$ W/cm^2 is presented in Table 1 and Fig. 2. Figure 2(a) shows the degree of reduction of scatters' intensities by introduction of the 0.6% bandwidth at normal and oblique incidences. It is seen that the reduction percentage of $3\omega/2$ and SBS scatters are not much changed while that of SRS is significantly reduced at oblique incidence, compared to those at normal incidence. Figure 2(b) shows the degree of changes in the scatters' intensities from normal incidence to oblique (30°) incidence, respectively, under narrowband and broadband conditions. It is seen that $3\omega/2$ and SRS scatters are enhanced while SBS scatters are weakened under both conditions, but the degree of changes is higher in the broadband case.

Table 1. The results of shots with ~ 230 J energies at normal and oblique incidences.

Laser type	Incidence type	Laser energy (J)	$3\omega/2$ intensity[a] (a.u.)	SBS energy[b] (J)	SRS energy[b] (mJ)
Narrowband	normal	220	1.7±0.3	6.9±1.4	21±4
Narrowband	oblique	241	4.4±0.7	3.4±0.7	43±9
Broadband	normal	226	0.4±0.1	3.0±0.6	5±1
Broadband	oblique	234	1.4±0.2	0.8±0.2	34±7

[a]Total intensity of the scatters at different angles, [b]backscatter energy within the full aperture of optics.

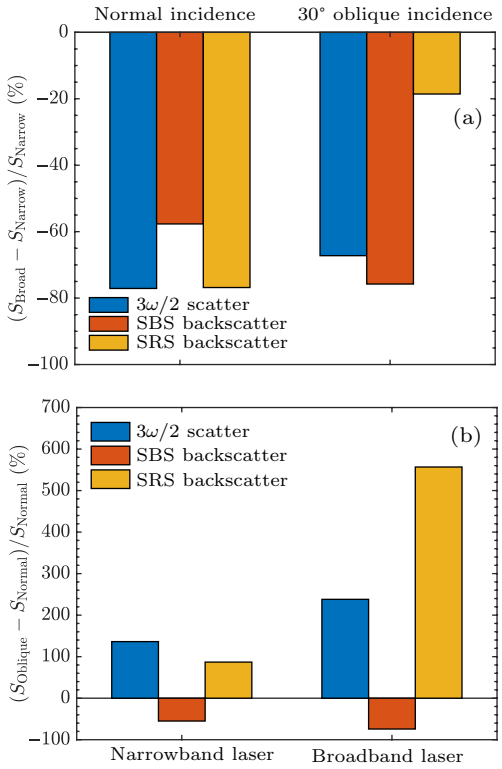


Fig. 2. Comparison of narrowband and broadband LPI-scatters at normal and oblique incidences with laser energy of ~ 230 J based on Table 1. Note the intensities of scatters being compared (S) are normalized to their corresponding incident laser energies to make them directly comparable. (a) The subscripts "Narrow" and "Broad" refer to the results obtained with narrowband and broadband lasers, respectively. (b) The subscripts "Oblique" and "Normal" refer to the results obtained at oblique and normal incidences, respectively.

Here we propose qualitative interpretations for the above observations. The reflectivity of SRS is higher with oblique incidence, which may be attributed to the fact that oblique incidence corresponds to lower laser absorption (as laser reflects at lower densities) and therefore lower temperature, which is in favor of the growth of SRS and TPD. For SBS, the reflected light previously included in the scatters no longer goes the backward path, resulting in a certain degree of reduction. There may be other possible explanations for the above results, but, most importantly, Table 1 and Fig. 2 confirm that the reduction of LPI-scatters by introduction of bandwidth persists within a certain range of incident angles, making broadband lasers applicable to the drive schemes that are not spherically symmetric (e.g., double-cone ignition).

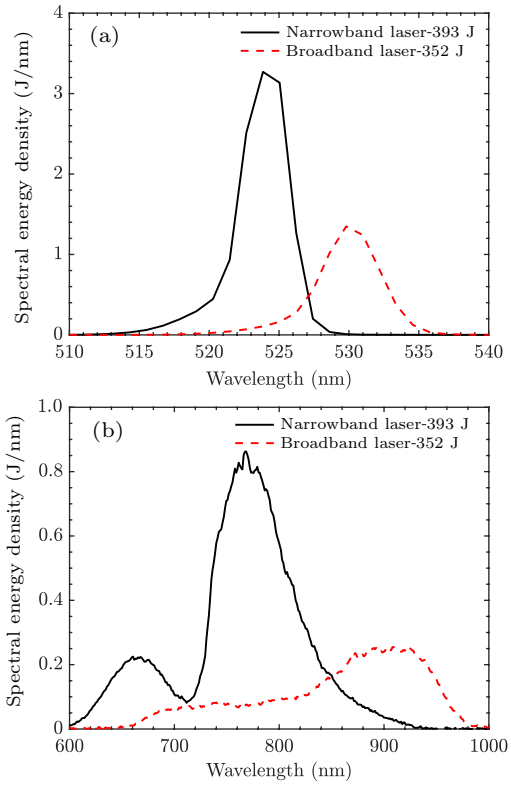


Fig. 3. Comparison of narrowband and broadband spectral distributions at normal incidence with laser energies of 350–400 J. (a) SBS backscatters. (b) SRS backscatters.

The reasons for the reduction of SBS and SRS backscatterings are thoroughly discussed in our previous work,[29] where SBS is directly mitigated by the bandwidth via the suppression of growth while SRS is indirectly affected by

the bandwidth via the mitigation of filamentation. Here, we present discussions on the differences in spectral distributions of the backscatters under monochromatic and broadband conditions. Figures 3(a) and 3(b) respectively show the spectra of SBS and SRS backscatters at 350–400 J at normal incidence, corresponding to average intensities of $\sim 4.6\times10^{14}$ W/cm^2.

Comparing the two spectra in Fig. 3(a), the narrowband SBS spectrum has a blueshift of about 2 nm relative to the laser center wavelength of 526.1 nm, and the strong region is in the range of 523–525 nm. In the broadband case, the strong region is 528–532 nm, indicating a small redshift to the center wavelength of 529.3 nm. According to the general theory of SBS backscattering,[2] the signal consists of three parts, namely, SBS scatters stimulated in the high-density region near the critical density ($n_{\rm cr}$), SBS scatters stimulated in the low-density region, and reflected laser. They attach different Doppler shifts due to the motion of plasma, so the measured wavelengths change relative to their original values. In general, the central wavelength of the low-density SBS is the smallest, then the reflected laser, and the largest is that of the high-density SBS. In the narrowband case, the measured spectrum is the superposition of the three, in which the spectral width reflects the wavelength difference from the low-density SBS to the high-density SBS with different Doppler frequency shifts, and the overall blueshift may imply that SBS mainly develops at underdense regions. In the broadband case, the small redshift may be explained by the self-cross beam energy transfer (self-CBET) between the various frequency components within the bandwidth, which was also observed in previous simulations.[32]

In the experimental configuration, the short-wavelength component of the incident light acts as the pump of CBET and the long-wavelength component of the backward light acts as the seed. The spatial rate of CBET energy gain is proportional to the resonance function $R(\eta)=\nu_{\rm a}^2|\eta|/\left[\left(\eta^2-1\right)^2+\nu_{\rm a}^2\eta^2\right]$ accounting for how closely the driven wave satisfies the dispersion relation,[33] which maximizes at $|\eta|\sim1$. Here $\nu_{\rm a}\sim0.2$ is the dimensionless amplitude damping rate for the ion acoustic wave for the CH plasma,[34] and η is calculated by the following formula:

$$\eta\approx9.7\times10^2\frac{\left[2\left(1-n_{\rm e}/n_{\rm cr}\right)\left(1-\cos\alpha\right)\right]^{1/2}\left(u/c\right)\cos\beta-\left(1-\lambda_{\rm pump}/\lambda_{\rm seed}\right)}{\left[2\left(1-n_{\rm e}/n_{\rm cr}\right)\left(1-\cos\alpha\right)\right]^{1/2}\left[\left(ZT_{\rm e,keV}+3T_{\rm i,keV}\right)/A\right]^{1/2}},\tag{1}$$

where $n_{\rm e}$ is the local electron density; u is the local flow velocity; c is the speed of light in vacuum; $\lambda_{\rm pump}$ and $\lambda_{\rm seed}$ are, respectively, the wavelengths of the pump and the seed; $T_{\rm e,keV}$ and $T_{\rm i,keV}$ are, respectively, the electron and ion temperatures in keV; $Z\sim3.5$ and $A\sim6.5$ are, respectively, the average ionization and the atomic number of CH plasma; $\alpha\sim180^\circ$ is the angle between the wavevectors of the pump and the seed; and $\beta\sim180^\circ$ is the angle between the wavevector of the ion acoustic wave and the flow velocity. A radiation hydrodynamics simulation using FLASH code[35,36] with a flux-limiter of 0.06 is performed to estimate the plasma conditions at 4.6×10^{14} W/cm^2, which could better fit the situation of CH plasmas at such intensity.[37,38] The results give a density scalelength of ~170 μm, an electron temperature of ~1 keV, and an ion temperature of ~0.5 keV for the averages at underdense plasmas. The scalelength is close to the spot size (180 μm), indicating that the free expansion of plasma into vacuum is limited by the small spot size, which makes the results relatively insensitive to the value of flux-limiter within a reasonable range. Take $n_{\rm e}\sim n_{\rm cr}/2$ and $u/c\sim0.0003$ for example, one obtains $\lambda_{\rm pump}/\lambda_{\rm seed}\sim0.9992$. For the $\lambda_{\rm pump}$ at the center wavelength of the incident laser (529.3 nm), the corresponding amplified $\lambda_{\rm seed}$ is ~529.7 nm, which is close to the small redshift observed in Fig. 3(a) under the broadband condition. Although the above calculation is rough due to the lack of precise diagnostics of plasma conditions, they still reveal the possibility of the self-CBET phenomenon.

In Fig. 3(b), the strongest peak of the SRS backscatter under the monochromatic condition is within the range of 720–860 nm, corresponding to the electron density from $0.07n_{\rm cr}$ to $0.15n_{\rm cr}$. Outside this range, the intensity is much lower, which is similar to the typical SRS backscatter spectral characteristics of an ultraviolet laser.[39] In the broadband case, the scattering region density is significantly expanded — the redshift edge is close to $0.25n_{\rm cr}$, and there is no obvious short cutoff usually believed to be related to the Landau damping. As mentioned earlier, SRS under the broadband condition is believed to be reduced by the mitigation of filamentation by the introduction of bandwidth. Then, the spectral distribution could be modified for the same reason. The threshold for filamentation instability induced by the ponderomotive force and thermal effects is estimated as[40]

$$I_{14}\left(n_{\rm e}/n_{\rm cr}\right)\geq4.4T_{\rm e,keV}/\left[H\left(f_{\#}\lambda_\mu\right)^2\right],\tag{2}$$

where I_{14} is the laser intensity in 10^{14} W/cm^2, λ_μ is the laser wavelength in microns, and $H\sim2$ is a factor to account for thermal effects. Substituting $T_{\rm e,keV}\approx1$, $I_{14}\approx4.6$, and $\lambda_\mu\approx0.53$ into the inequality, we get $n_{\rm e}/n_{\rm cr}\geq0.1$, which means that the filament could start to form at $\sim n_{\rm cr}/10$. The peak wavelength of the measured SRS spectrum in the monochromatic case is ~770 nm, which roughly corresponds to $\sim n_{\rm cr}/10$. Thus, filamentation in the monochromatic case enhances localized light intensity at underdense plasma and makes SRS spectrum present peaks at short wavelengths.

In addition to the SBS and SRS spectra, the characteristics of $3\omega/2$ spectra are also worth discussing. Here, $3\omega/2$ is measured to gain insight into the behavior of TPD, which is a result of Thomson up-scattering of the incident laser light off TPD-produced plasmons.[41] The redshift peak of the measured $3\omega/2$ spectra may also be produced by absolute SRS in addition to TPD, which probably does not make much practical difference because in both cases the instability saturates into Langmuir turbulence that spans the $n_{cr}/4$ region.

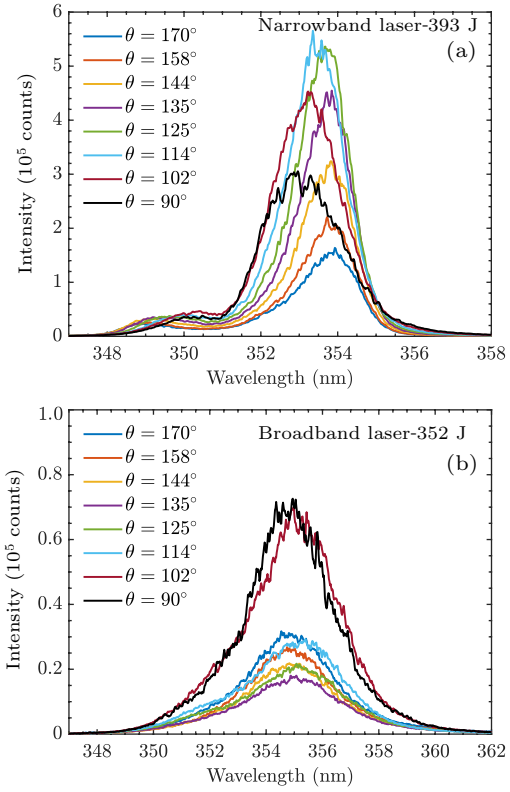


Fig. 4. Spectral distributions of $3\omega/2$ at normal incidence with laser energies of 350–400 J. (a) Obtained with the narrowband laser. (b) Obtained with the broadband laser.

Figure 4 shows the variation of the $3\omega/2$ spectra at scattering angles (θ) of 90°–170° . Under the narrowband condition, the spectrum at each angle in Fig. 4(a) shows a two-peak distribution around $2\lambda_0/3$ ($\sim$ 350.7 nm, here λ_0 refers to the center wavelength of laser), in which the redshift peak's intensity is higher and its frequency shift is larger than those of the blueshift peak. The two-peak distribution can be intuitively explained by the nature of TPD — two electron plasma waves (EPWs) generated by TPD have a small frequency difference, so the scattered light generated by them after coupling incident light waves will certainly have a small wavelength difference. The peak intensities and frequency shifts at these angles are different — the larger the scattering angle, the smaller the frequency shift, and the strongest scattering is at $\sim 120°$, which is similar to those measured with ultraviolet lasers.[42] Theoretically, Thomson up-scattering of a laser at normal incidence onto a density gradient off the red-shifted EPW from TPD is expected to occur at $\theta = 111°$,[43] which is roughly consistent with the measurements. Based on the matching conditions for TPD and the Thomson up-scattering, one has

$$\Delta\lambda_R/\lambda_0 \approx T_{e,keV}\,(2.94 - 3.20\cos\theta) \times 10^{-3}, \tag{3}$$

where $\Delta\lambda_R$ is the wavelength difference between the redshift peak and $2\lambda_0/3$. It is seen that the magnitude of the wavelength difference is related to the plasma temperature and the scattering angle, so the wavelength differences measured at those angles are various, which is consistent with the experimental results. For $\lambda_R \sim 353.7$ nm at 125°, one gets $T_e \sim 1.2$ keV at $\sim n_{cr}/4$, which is a bit higher than the average temperature over the underdense plasmas obtained by the simulation. The reason for this is possibly that the measured $\Delta\lambda_R$ is slightly modified by the Doppler effect induced by the plasma motion.

Under the broadband condition, the spectra have a one-peak distribution, as shown in Fig. 4(b). The center wavelength of the peak is about 535 nm, so the redshift is ~ 2 nm relative to $2\lambda_0/3$ ($\sim$ 352.9 nm, note the center wavelengths of narrowband and broadband lasers are different), and the change of the center wavelength is not obvious over angles. One simple speculation could be that absolute SRS dominates the production of $3\omega/2$ under the broadband condition, which is different from the TPD dominance under the monochromatic condition. This speculation can be checked by the following calculation of thresholds of absolute SRS and TPD under broadband conditions:[25]

$$I_{14,aSRS} \approx 1.2 \times 10^3 L_\mu^{-1} \lambda_\mu^{-1} (\Delta\omega/\omega_0)^{1/3}, \tag{4}$$

$$I_{14,TPD} \approx 4.1 \times 10^2 T_{e,keV}^{3/4} L_\mu^{-2/3} \lambda_\mu^{-4/3} (\Delta\omega/\omega_0)^{1/2}, \tag{5}$$

when the bandwidth fits a Lorentzian function. Here $I_{14,aSRS}$ and $I_{14,TPD}$ are the threshold intensities in 10^{14} W/cm^2, respectively, for absolute SRS and TPD, and L_μ is the density scale-length in microns. Substituting $\Delta\omega/\omega_0 \approx 0.6\%$, $L_\mu \approx 170$, $T_{e,keV} \approx 1$, and $\lambda_\mu \approx 0.53$ into the above formulas, we get $I_{14,aSRS} \approx I_{14,TPD} \approx 2.4$, which corresponds to an incident laser energy of about 200 J. Considering the laser absorption in the underdense region and the localized intense speckles within the laser spot induced by CPP, the threshold energy could be more or less. For instance, a three times more intense speckle could reduce the threshold energy to a level below 100 J, which is consistent with our measurements that $3\omega/2$ existed at $\sim$ 100 J in both the monochromatic and the broadband cases.[29] The most intense speckle could be about five times more intense than the average intensity, but the number of speckles at such intensity is usually very small, and speckles at two to three times the average intensity should be more common. Anyhow, the 0.6% bandwidth itself is not large enough to make the threshold for either absolute SRS or TPD higher than the laser intensity, so the observed reduction of $3\omega/2$ is more likely to be attributed to the mitigation of laser filaments,

similar to the reason for the reduction of SRS. Since the effect of filamentation mitigation should be similar for both absolute SRS and TPD as they develop at the same plasma region ($n_{cr}/4$), the speculation of different sources of $3\omega/2$ under the two bandwidths is unlikely.

Here we propose another speculation on the reason for the one-peak distribution of $3\omega/2$ under the broadband condition — spectral mixing of different frequency components within the bandwidth, which is on the assumption that the main sources of $3\omega/2$ under the conditions of the two bandwidths are TPD. In Fig. 5(a), an example of spectral mixing is given by dividing the laser bandwidth into nine sub-bands at a wavelength interval of 1 nm, and the energies of the sub-bands are given in Fig. 1(b). Since the laser energy of any sub-band is low, we assume the $3\omega/2$ spectrum of each sub-band is similar to the shape of that in a $\sim$ 100 J narrowband case (minimal energy shot in the experiments), and the reason why $3\omega/2$ could still be produced at such low energy could be attributed to the intense laser speckles, as discussed earlier. The center wavelength of $3\omega/2$ stimulated by each sub-band is determined by the center of the laser spectrum of the sub-band relative to the center wavelength of the narrowband laser. The intensity of $3\omega/2$ stimulated by each sub-band is assumed to change linearly according to the ratio of its laser energy to the $\sim$ 100 J narrowband energy with an additional 80% reduction accounted for the reduction in integrated intensity in the broadband cases. Since the broadband laser consists of those sub-bands, its $3\omega/2$ spectrum is then artificially treated as the linear superposition of $3\omega/2$ spectra produced by those sub-bands, giving a one-peak spectrum (black-dashed curve) that looks similar in intensity and shape to the measured $3\omega/2$ spectrum produced by the broadband light itself (black-solid curve). Since the wavelength shift between the two peaks should also be related to the energy, it is reasonable that the calculated spectrum is not exactly the same as the measured one.

In the above treatment, we only (for simplicity) divide the laser that stimulates the EPWs into sub-bands but the light coupled with the EPWs remains whole, which should not be the case because both the light waves are the incident laser. If the light waves in the two processes (namely, EPW production and coupling) are both divided into sub-bands, then it will give a squared number of sub-spectra to be added up, which is too many to be presented as a simple example. Nevertheless, one can intuitively imagine that in this case the added spectrum would have a smoother and wider profile compared to the presented one. It should be noted that the treatment of sub-bands is only an attempt to visually reproduce the one-peak $3\omega/2$ distribution in the broadband case from the two-peak distributions in the monochromatic cases, so the results may not reflect the actual physical mechanism because one may argue that the various frequency bands are not likely to act independently in practice given that the unstable region broadens dramatically in the nonlinear turbulent stage, in which case the sub-band treatment of the coupling process may still be valid but that of the EPW production is not.

In addition to the spectral shape, the angular distribution of $3\omega/2$ in the broadband case is also different from that in the narrowband case. In Fig. 5(b), the angular distributions of $3\omega/2$ in the two cases are compared, which shows that the broadband is more concentrated at the small scattering angle than the narrow band. If we treat a scattering range of 90°–120° as side-scattering, the ratio of $3\omega/2$ side-scattering to the total intensity is $\sim$ 57% in the broadband case, which is higher than that in the narrowband case ($\sim$ 47%). Since the EPW corresponding to side-scattering is also side-propagating, the probability of preheating by the hot electrons produced by a side-propagating EPW should be lower than that produced by a forward-propagating EPW, so a larger proportion of side-scattering induced by the bandwidth may be not that harmful to the preheating control.

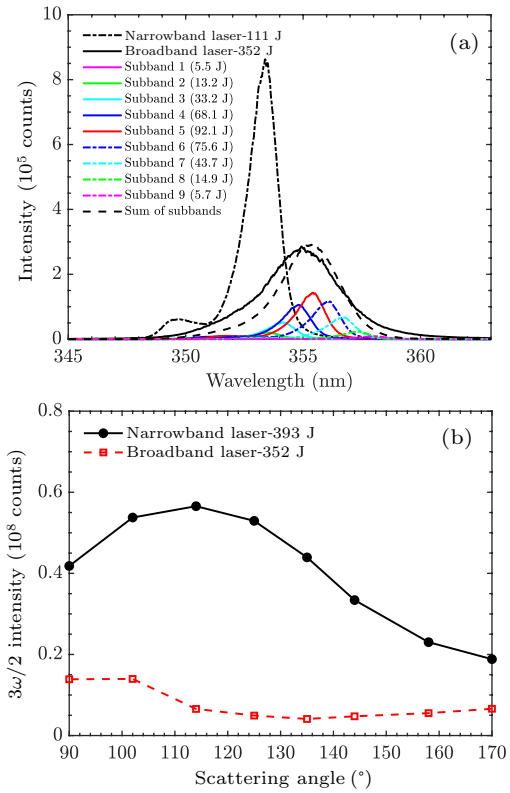


Fig. 5. Analyses of the spectral distributions of $3\omega/2$. (a) Subband treatment of $3\omega/2$ in the broadband case. (b) $3\omega/2$ angular distributions in the narrowband and broadband cases.

4. Conclusion and perspectives

Experimental results regarding the spectral characteristics of LPIs with broadband laser are reported and discussed. First, the reduction of LPI-scatters by introduction of bandwidth was observed to persist within a certain range of incident angles. In addition to the reduction of intensities, the spectral distributions of the scatters were also changed under the broadband condition with respect to the narrowband case. SBS backscatter has a small redshift in the broadband case contrary to the

blueshift with narrowband laser, which may be explained by the self-cross beam energy transfer between the various frequency components within the bandwidth. SRS backscatter spectrum presents a peak at a longer wavelength in the broadband case compared to the short one in the narrowband case, which is possibly attributed to the mitigation effect of bandwidth on filaments at underdense plasmas. $3\omega/2$ has a one-peak distribution in the spectrum under the broadband condition, which is different from the two-peak distribution under the narrowband condition, and the reason may be related to the spectral mixing of different frequency components within the bandwidth if the sources of the two are both TPD. Since the spectral characteristics of scatters are closely related to the actual physical processes during the laser–plasma interactions, the reported spectra could be informative to the understanding of broadband LPIs, as well as the benchmark of simulation codes used to evaluate the effects of laser bandwidth in DDICF.

Acknowledgement

Project supported by the National Natural Science Foundation of China (Grant No. 11905280).

References

[1] Nuckolls J, Thiessen A, Wood L and Zimmerman G 1972 *Nature* **239** 139
[2] Craxton R S, Anderson K S, Boehly T R, Goncharov V N, Harding D R, Knauer J P, McCrory R L, McKenty P W, Meyerhofer D D, Myatt J F, Schmitt A J, Sethian J D, Short R W, Skupsky S, Theobald W, Kruer W L, Tanaka K, Betti R, Collins T J B, Delettrez J A, Hu S X, Marozas J A, Maximov A V, Michel D T, Radha P B, Regan S P, Sangster T C, Seka W, Solodov A A, Soures J M, Stoeckl C and Zuegel J D 2015 *Phys. Plasmas* **22** 110501
[3] Rosenbluth M N, White R B and Liu C S 1973 *Phys. Rev. Lett.* **31** 1190
[4] Kruer W 2003 *The Physics of Laser Plasma Interactions* (Boca Raton: CRC Press) pp. 73–94
[5] Yan R, Ren C, Li J, Maximov A V, Mori W B, Sheng Z M and Tsung F S 2012 *Phys. Rev. Lett.* **108** 175002
[6] Igumenshchev I V, Seka W, Edgell D H, Michel D T, Froula D H, Goncharov V N, Craxton R S, Divol L, Epstein R, Follett R, Kelly J H, Kosc T Z, Maximov A V, McCrory R L, Meyerhofer D D, Michel P, Myatt J F, Sangster T C, Shvydky A, Skupsky S and Stoeckl C 2012 *Phys. Plasmas* **19** 056314
[7] Laval G, Pellat R, Pesme D, Ramani A, Rosenbluth M N and Williams E A 1977 *Phys. Fluids* **20** 2049
[8] Thomson J J and Karush J I 1974 *Phys. Fluids* **17** 1608
[9] Obenschain S P, Luhmann N C and Greiling P T 1976 *Phys. Rev. Lett.* **36** 1309
[10] Mostovych A N, Obenschain S P, Gardner J H, Grun J, Kearney K J, Manka C K, McLean E A and Pawley C J 1987 *Phys. Rev. Lett.* **59** 1193
[11] Bates J W, Myatt J F, Shaw J G, Follett R K, Weaver J L, Lehmberg R H and Obenschain S P 2018 *Phys. Rev. E* **97** 061202
[12] Marozas J A, Hohenberger M, Rosenberg M J, Turnbull D, Collins T J B, Radha P B, McKenty P W, Zuegel J D, Marshall F J, Regan S P, Sangster T C, Seka W, Campbell E M, Goncharov V N, Bowers M W, Di Nicola J M G, Erbert G, MacGowan B J, Pelz L J and Yang S T 2018 *Phys. Rev. Lett.* **120** 085001
[13] Lu L 1989 *Phys. Fluids B* **1** 1605
[14] Zhao Y, Weng S, Chen M, Zheng J, Zhuo H, Ren C, Sheng Z and Zhang J 2017 *Phys. Plasmas* **24** 112102
[15] Follett R K, Shaw J G, Myatt J F, Palastro J P, Short R W and Froula D H 2018 *Phys. Rev. Lett.* **120** 135005
[16] Guzdar P N, Liu C S and Lehmberg R H 1993 *Phys. Fluids B* **5** 910
[17] Weaver J, Lehmberg R, Obenschain S, Kehne D and Wolford M 2017 *Appl. Opt.* **56** 8618
[18] Obenschain S P, Schmitt A J, Bates J W, Wolford M F, Myers M C, McGeoch M W, Karasik M and Weaver J L 2020 *Philos. Trans. R. Soc. A* **378** 20200031
[19] Gao Y, Cui Y, Ji L, Rao D, Zhao X, Li F, Liu D, Feng W, Xia L, Liu J, Shi H, Du P, Liu J, Li X, Wang T, Zhang T, Shan C, Hua Y, Ma W, Sun X, Chen X, Huang X, Zhu J, Pei W, Sui Z and Fu S 2020 *Matter Radiat. Extremes* **5** 065201
[20] Zhou H Y, Xiao C Z, Zou D B, Li X Z, Yin Y, Shao F Q and Zhuo H B 2018 *Phys. Plasmas* **25** 062703
[21] Ma H H, Li X F, Weng S M, Yew S H, Kawata S, Gibbon P, Sheng Z M and Zhang J 2021 *Matter Radiat. Extremes* **6** 055902
[22] Yi S Y, Zhou H Y, Jiao J L, Wang H Z, Yan R, Zhang P D and Yin Y 2023 *Plasma Phys. Controlled Fusion* **65** 065005
[23] Wen H, Follett R K, Maximov A V, Froula D H, Tsung F S and Palastro J P 2021 *Phys. Plasmas* **28** 042109
[24] Seaton A G, Yin L, Follett R K, Albright B J and Le A 2022 *Phys. Plasmas* **29** 042707
[25] Follett R K, Shaw J G, Myatt J F, Dorrer C, Froula D H and Palastro J P 2019 *Phys. Plasmas* **26** 062111
[26] Follett R K, Shaw J G, Myatt J F, Wen H, Froula D H and Palastro J P 2021 *Phys. Plasmas* **28** 032103
[27] Liu Q K, Zhang E H, Zhang W S, Cai H B, Gao Y Q, Wang Q and Zhu S P 2022 *Phys. Plasmas* **29** 102105
[28] Gao Y, Ji L, Zhao X, Cui Y, Rao D, Feng W, Xia L, Liu D, Wang T, Shi H, Li F, Liu J, Du P, Li X, Liu J, Zhang T, Shan C, Hua Y, Ma W, Sui Z, Zhu J, Pei W, Fu S, Sun X and Chen X 2020 *Opt. Lett.* **45** 6839
[29] Lei A, Kang N, Zhao Y, Liu H, An H, Xiong J, Wang R, Xie Z, Tu Y, Xu G, Zhou X, Fang Z, Wang W, Xia L, Feng W, Zhao X, Ji L, Cui Y, Zhou S, Liu Z, Zheng C, Wang L, Gao Y, Huang X and Fu S 2024 *Phys. Rev. Lett.* **132** 035102
[30] Cui Y, Gao Y, Rao D, Liu D, Li F, Ji L, Shi H, Liu J, Zhao X, Feng W, Xia L, Liu J, Li X, Wang T, Ma W and Sui Z 2019 *Opt. Lett.* **44** 2859
[31] Ji L, Zhao X, Liu D, Gao Y, Cui Y, Rao D, Feng W, Li F, Shi H, Liu J, Li X, Xia L, Wang T, Liu J, Du P, Sun X, Ma W, Sui Z and Chen X 2019 *Opt. Lett.* **44** 4359
[32] Follett R K, Colaitis A, Seaton A G, Wen H, Turnbull D, Froula D H and Palastro J P 2023 *Phys. Plasmas* **30** 042102
[33] Edgell D H, Follett R K, Igumenshchev I V, Myatt J F, Shaw J G and Froula D H 2017 *Phys. Plasmas* **24** 062706
[34] Williams E A, Berger R L, Drake R P, Rubenchik A M, Bauer B S, Meyerhofer D D, Gaeris A C and Johnston T W 1995 *Phys. Plasmas* **2** 129
[35] Fryxell B, Olson K, Ricker P, Timmes F X, Zingale M, Lamb D Q, MacNeice P, Rosner R, Truran J W and Tufo H 2000 *Astrophys. J. Suppl. Ser.* **131** 273
[36] Dubey A, Antypas K, Ganapathy M K, Reid L B, Riley K, Sheeler D, Siegel A and Weide K 2009 *Parallel Comput.* **35** 512
[37] Delettrez J 1986 *Can. J. Phys.* **64** 932
[38] Smalyuk V A, Hu S X, Goncharov V N, Meyerhofer D D, Sangster T C, Stoeckl C and Yaakobi B 2008 *Phys. Plasmas* **15** 082703
[39] Kang N, Liu H Y, Zhao Y, Ji S Z, Zhou S L and Lei A L 2020 *Plasma Phys. Controlled Fusion* **62** 055007
[40] Montgomery D S, Moody J D, Baldis H A, Afeyan B B, Berger R L, Estabrook K G, Lasinski B F, Williams E A and Labaune C 1996 *Phys. Plasmas* **3** 1728
[41] Seka W, Edgell D H, Myatt J F, Maximov A V, Short R W, Goncharov V N and Baldis H A 2009 *Phys. Plasmas* **16** 052701
[42] Kang N, Liu H, Lin Z, Lei A, Zhou S, Fang Z, An H, Li K and Fan W 2017 *Plasma Phys. Controlled Fusion* **59** 105011
[43] Michel P 2023 *Introduction to Laser-Plasma Interactions* (Gewerbestrasse: Springer Nature Switzerland AG) pp. 293–296